

COMMUNICATION

Quantifying the Effects of Quadrupolar Sink via ^{15}N Relaxation Dynamics in Metronidazoles Hyperpolarized via SABRE-SHEATH

Received 00th January 20xx,
Accepted 00th January 20xx

DOI: 10.1039/x0xx00000x

Jonathan R. Birchall,^a Mohammad S. H. Kabir,^a Oleg G. Salnikov,^{b,c,d} Nikita V. Chukanov,^{b,c} Alexandra Svyatova,^{b,c} Kirill V. Kovtunov,^{b,c} Igor V. Koptyug,^{b,c} Juri G. Gelovani,^{a,e} Boyd M. Goodson,^f Wellington Pham,^g and Eduard Y. Chekmenev^{a,h*}

^{15}N spin-lattice relaxation dynamics in metronidazole- $^{15}\text{N}_3$ and metronidazole- $^{15}\text{N}_2$ isotopologues are studied for rational design of ^{15}N -enriched biomolecules for Signal Amplification by Reversible Exchange in microtesla fields. ^{15}N relaxation dynamics mapping reveals the deleterious effects of interactions with polarization transfer catalyst and quadrupolar ^{14}N nucleus within the spin-relayed ^{15}N - ^{15}N network.

The nuclear spin polarization P at thermal equilibrium is governed by a Boltzmann distribution of nuclear spins among Zeeman energy levels. P increases linearly with magnetic field strength. For a conventional high-field NMR spectrometer (e.g., 9.4 T) or clinical Magnetic Resonance Imaging (MRI) scanner (e.g., 3 T) at room temperature, P is typically on the order of 10^{-5} to 10^{-6} , resulting in a relatively low sensitivity of NMR-based applications. For NMR applications where this sensitivity is too low to be useful, various hyperpolarization strategies may be employed to increase P by as much as 4-5 orders of magnitude,^{1,2} with corresponding signal gains.

One such technique is Signal Amplification by Reversible Exchange (SABRE), pioneered by Duckett *et al.* in 2009,³ which utilizes simultaneous reversible chemical exchange of

parahydrogen (p-H₂) and to-be-hyperpolarized substrate molecules at a metal center. In SABRE, the transfer of nuclear spin polarization from parahydrogen-derived hydrides to a spin-polarizable substrate occurs spontaneously via the network of spin-spin couplings established in a transient polarization transfer catalyst (PTC) complex (Figure 1a).³⁻⁵ While several approaches have been developed for polarization transfer in SABRE,⁶⁻¹¹ a variant of SABRE, SABRE-SHEATH (SABRE in SHield Enables Alignment Transfer to Heteronuclei),^{12,13} facilitates the generation of highly polarized spin states of heteronuclei¹⁴⁻¹⁷ including nitrogen-15 with high polarization ($P_{^{15}\text{N}} > 30\%$)¹⁸ persisting for tens of minutes.¹⁹ Nitrogen is found in a wide range of biomolecules including nucleic acids, amino acids, proteins, and drugs. Since SABRE-SHEATH is performed at very low magnetic fields (< 1 μT) and near room temperature, the production of such HP ^{15}N spin-labeled biomolecules is comparatively simple, fast and inexpensive.¹⁰

Nitroimidazoles can be readily reduced in anaerobic environments. This property has been widely employed in a number of antibiotic drugs,²⁰ Positron Emission Tomography (PET) tracers for hypoxia sensing,²¹ and also in a number of emerging cancer therapeutics: e.g., evofosfamide (a.k.a. TH-302)²² and the radiosensitizer nimorazole.²³

Metronidazole is an FDA-approved antibiotic,²⁴ belonging to the nitroimidazole class of compounds. We envision that ^{15}N -hyperpolarized metronidazole can be potentially employed for hypoxia sensing in a manner similar to that of nitroimidazole-based Positron Emission Tomography (PET) tracers. One such tracer, ¹⁸F-fluoromisonidazole (FMISO),²¹ undergoes reduction in hypoxic environment (including most notably hypoxic tumors) and the metabolic products of this reduction process become trapped in hypoxic cells, providing contrast in FMISO PET images.²⁵ The enormous potential for using HP MRI to sense metabolic transformations *in vivo* has been well demonstrated^{10,26}; correspondingly, HP MRI of metronidazole may obviate the limitations of FMISO PET imaging, including the use of ionizing radiation, the requirement for long clearance time from surrounding tissues, and the inability to spectrally

^a Department of Chemistry, Integrative Biosciences (Ibio), Wayne State University, Karmanos Cancer Institute (KCI), Detroit, Michigan 48202, United States. E-mail: chekmenevlab@gmail.com

^b International Tomography Center, SB RAS, 3A Institutskaya St., Novosibirsk 630090, Russia

^c Novosibirsk State University, 2 Pirogova St., Novosibirsk 630090, Russia

^d Boreskov Institute of Catalysis SB RAS, 5 Acad. Lavrentiev Pr., Novosibirsk 630090, Russia

^e United Arab Emirates University, Al Ain, United Arab Emirates

^f Department of Chemistry and Biochemistry and Materials Technology Center, Southern Illinois University, Carbondale, Illinois 62901, United States

^g Vanderbilt University Institute of Imaging Science (VUIIS), Department of Radiology, Vanderbilt University Medical Center (VUMC), Department of Biomedical Engineering, Vanderbilt University, Vanderbilt-Ingram Cancer Center (VICC), Nashville, Tennessee 37232-2310, United States

^h Russian Academy of Sciences, Leninskiy Prospekt 14, Moscow, 119991, Russia

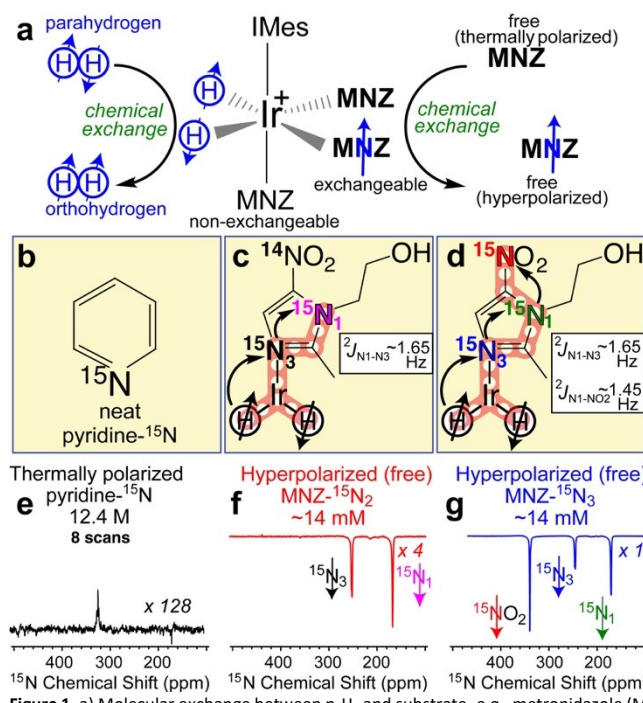
† To the memory of Dr. Kirill V. Kovtunov (PhD, 1983-2020), friend, colleague, and mentor.

Electronic Supplementary Information (ESI) available: Numerical values of ^{15}N polarization build-up and polarization decay constants, additional experimental details (file type, PDF). See DOI: 10.1039/x0xx00000x

distinguish parent compounds from downstream products. We have demonstrated efficient SABRE-SHEATH hyperpolarization of the $^{15}\text{N}_3$ site in natural abundance metronidazole with $\%P_{15\text{N}}$ exceeding 30%.¹⁸ This nitrogen site directly interacts with the PTC, and therefore gains its polarization directly from p-H₂-derived hydrides. Subsequently, commercially available metronidazole- $^{15}\text{N}_2\text{-}^{13}\text{C}_2$ (Sigma-Aldrich, #32744) was employed for SABRE-SHEATH, but unfortunately yielded significantly lower $\%P_{15\text{N}}$ (roughly by an order of magnitude), although all ^{15}N - and ^{13}C -labeled sites have been successfully hyperpolarized.^{27, 28} Most recently we have synthesized metronidazole- $^{15}\text{N}_3$ and demonstrated $^{15}\text{N}\rightarrow^{15}\text{N}$ spin-relayed SABRE-SHEATH hyperpolarization via two-bond $^{15}\text{N}\text{-}^{15}\text{N}$ spin-spin couplings, Figure 1d. This metronidazole- $^{15}\text{N}_3$ isotopologue exhibited a remarkable $\%P_{15\text{N}}$ of ~16% on all three ^{15}N sites including $^{15}\text{NO}_2$, which has a polarization relaxation decay constant T_1 approaching 10 minutes. However, in order to facilitate more effective production of HP biomolecules for bioimaging applications, it is clearly necessary to gain improved understanding of the underlying spin-relaxation phenomena to inform the rational design of these promising imaging agents. Here, we report a quantitative study of spin relaxation dynamics of metronidazole- $^{15}\text{N}_2$ and metronidazole- $^{15}\text{N}_3$ isotopologues, Figure 1c and Figure 1d respectively, using previously described experimental setup (Figure S2).^{27, 29} Catalyst activation was performed for approximately 2 h for each sample studied to ensure reproducibility, see Figure S1 in the Supporting Information (SI). Other experimental parameters (temperature, p-H₂ pressure, flow rate and in-shield magnetic field) were optimized for each isotopologue, Figure S1. Using an overpressure of 94 psig, p-H₂ was bubbled through a solution of MNZ ^{15}N -isotopologue substrate and Ir-IMes catalyst in 0.6 mL methanol-d₄ for one minute to facilitate polarization transfer in microtesla fields. Following polarization build-up, the sample solution was rapidly transferred (2-4 s to minimize the relaxation losses) to a 1.4 T NMR Pro (Nanalysis, Canada) benchtop NMR spectrometer for ^{15}N NMR detection (Figure 1h). Each relaxation/build-up curve was obtained by varying the time duration that the sample spent in a given magnetic field.

The key results related to ^{15}N T_1 relaxation at the optimal magnetic field during the SABRE-SHEATH polarization transfer process (*ca.* 0.4 μT , Figure S1) for metronidazole- $^{15}\text{N}_3$ and metronidazole- $^{15}\text{N}_2$ are shown in Figures 2e and 2f, respectively. As expected for microtesla magnetic fields, all ^{15}N sites within a given molecule share approximately the same relaxation rate (*e.g.*, 13.8-15.4 s for MNZ- $^{15}\text{N}_3$, Figure 2e). However, the $^{15}\text{NO}_2$ group replacement by $^{14}\text{NO}_2$ leads to dramatic, 3-fold shortening of the ^{15}N T_1 (4.3-4.8 s corresponding T_1 values for MNZ- $^{15}\text{N}_2$, Figure 2f). This striking effect can be explained by the enhanced scalar relaxation of the second kind^{30, 31} induced by the quadrupolar $^{14}\text{NO}_2$ site within the N-N spin-spin coupling network. These results are further supported by the overall similar ^{15}N T_1 trend at the Earth's magnetic field (*ca.* 10 μT in the basement of our lab at Detroit, MI, Table S1). Moreover, we find that each ^{15}N polarization build-up constant (T_b , Figure 2c and Figure 2d) at 0.4 μT is closely correlated with the corresponding T_1 value. In practice, this means that the increased relaxation

rate caused by the presence of the quadrupolar ^{14}N spin in MNZ- $^{15}\text{N}_2$ (despite the peripheral position of the NO_2 group) allows for achieving the steady-state $\%P_{15\text{N}}$ faster on $^{15}\text{N}_3$ and $^{15}\text{N}_1$ sites—but at significantly lower levels. The correlation plot of $\%P_{15\text{N}}$ versus T_1 at 0.4 μT indeed exhibits a linear trend with $R^2>0.99$ (Figure 2inset). When the magnetic field is sufficiently high (*e.g.*, 1.4 T, Figure 2g and Figure 2h), the increased frequency dispersion of the nuclear spins puts them in a weakly coupled regime with ^{15}N sites having significantly longer T_1 decay constants—on the order of many minutes.



On another note, the realization that scalar-coupled ^{14}N spins are highly deleterious in the context of SABRE-SHEATH suggests that if these quadrupolar effects would have been avoided, near-unity $P_{15\text{N}}$ would have been potentially achievable in the previous studies.¹⁸

It should be pointed out that substrate exchange of Ir-IMes catalyst may act as the potential source of additional undesirable ^{15}N relaxation (*e.g.*, due to compounding effects of quadrupolar Ir nucleus and the chemical exchange process).¹³ Consequently, a series of control experiments were performed, where the catalyst concentration was systematically varied from 0.5 mM to 1 mM to 2 mM at a fixed concentration of metronidazole isotopologue (Figures S3a-d). The [catalyst] increase from 0.5 mM to 2 mM results in a stepwise decrease in ^{15}N T_1 and T_b by approximately 2-fold at 0.4 μT (Figure S3b and Figure S3c). However, because the interplay of T_1 relaxation and catalyst concentration is complex in the SABRE process,^{32, 33} these decreases in ^{15}N T_1 and T_b at 0.4 μT are offset by the

overall increased catalyst-to-substrate ratio (*i.e.*, better substrate access to p-H₂ spin bath), resulting in somewhat greater %P_{15N} in metronidazole-¹⁵N₃ and similar %P_{15N} in metronidazole-¹⁵N₂ at higher [catalyst], Figure S3d. Of note, the Ir-IMes catalyst decreases ¹⁵N T₁ even at high magnetic fields (1.4 T, weakly coupled regime) for ¹⁵NO₂ (Figure S3a). Moreover, this observation clearly indicates a second reason (beyond agent purification) that SABRE catalyst removal^{18, 34-36} is warranted as soon polarization build-up is completed to minimize ¹⁵N polarization losses prior to biomedical utilization of HP metronidazole-¹⁵N₃ as a contrast agent.

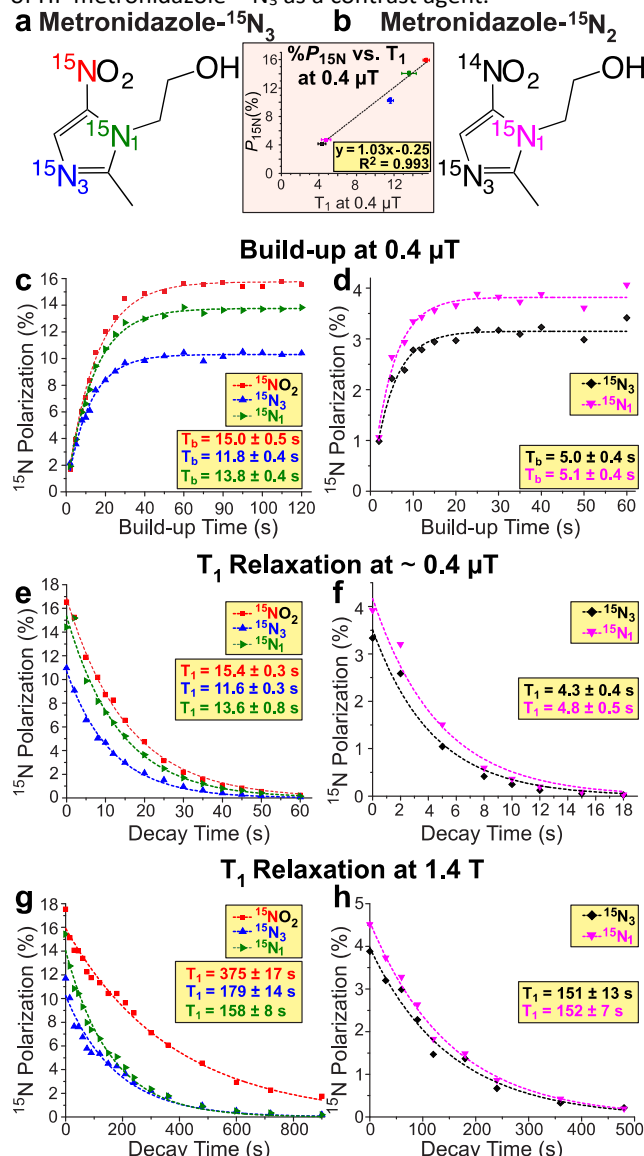


Figure 2. a-b) Structures of two metronidazole ¹⁵N-isotopologues. c-d) Corresponding ¹⁵N polarization build-up curves at 0.4 μ T. e-f) Corresponding ¹⁵N T₁ decay curves at 0.4 μ T. g-h) Corresponding ¹⁵N T₁ decay curves at 1.4 T. The presented data was recorded using a 2 mM IrIMes catalyst concentration and a corresponding 20 mM MNZ isotopologue concentration. All experiments are performed in CD₃OD.

The high levels of ¹⁵N polarization obtained in ¹⁵N-labeled metronidazole isotopologues enable direct ¹⁵N MRI. Figure 3 demonstrates the 2D ¹⁵N projection images of 5 mm NMR tubes filled with HP solutions of ¹⁵N-labeled metronidazole

isotopologues with the highest spatial resolution reported to date to the best of our knowledge.

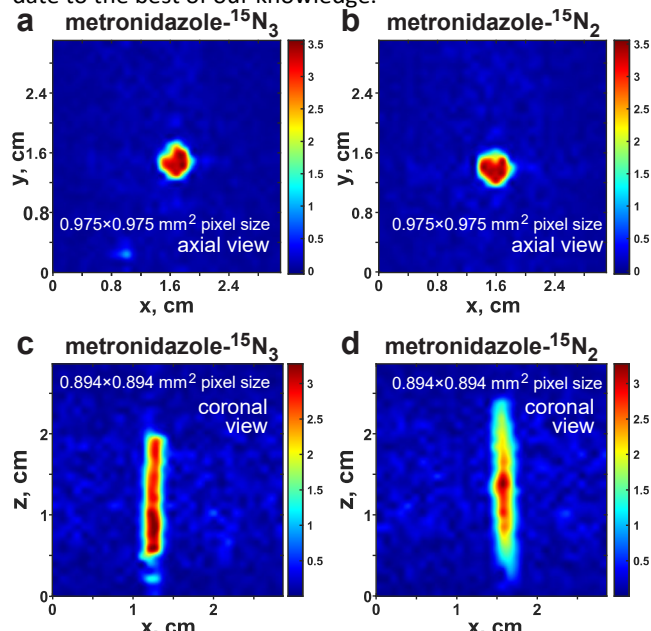


Figure 3. ¹⁵N MRI of 5 mm NMR tubes filled with hyperpolarized solutions of 0.1 M metronidazole-¹⁵N₃ (MNZ-¹⁵N₃) and metronidazole-¹⁵N₂ (MNZ-¹⁵N₂) respectively using 5 mM of Ir(COD)(Mes)Cl in methanol-d₄ obtained by TrueFISP pulse sequence. Imaging parameters employed: TR = 62.5 ms, TE = 3.6 ms, scan time = 2.0 seconds, flip angle = 15°, matrix size = 32 × 32 (zero-filled to 512 × 512). a) axial projection 2D image of metronidazole-¹⁵N₃ using 1 average (maximum SNR(SNR_{MAX}) is ~500), b) axial projection 2D image of metronidazole-¹⁵N₂ using 1 average, SNR_{MAX} is ~410, c) coronal projection 2D image of metronidazole-¹⁵N₃ using 8 averages, SNR_{MAX} is ~450, d) coronal projection 2D image of metronidazole-¹⁵N₂ using 8 averages, SNR_{MAX} is ~340.

Conclusions

In summary, the spin-relayed SABRE-SHEATH hyperpolarization approach allows efficient polarization of scalar coupled ¹⁵N-¹⁵N spin networks. These networks may be created via two-bond ¹⁵N-¹⁵N J-couplings at most. The presence of ¹⁴N spins in such networks must be avoided to prevent deleterious polarization losses due to quadrupolar relaxation effects (manifested on ¹⁵N as scalar relaxation of the second kind¹⁶), in order to maximize the resulting %P_{15N}. Although the catalyst decreases the ¹⁵N spin-relaxation time constant, T₁, of metronidazole isotopologues in the microtesla regime in a concentration-dependent manner, the overall impact on the achievable ¹⁵N polarization level is relatively minor. On the other hand, the presence of a ¹⁴N nucleus in the scalar coupling network results in an approximately 3-fold decrease of microtesla ¹⁵N T₁ values for all ¹⁵N sites in the ¹⁵N₂-isotopologue versus the ¹⁵N₃-isotopologue over a wide range of catalyst concentrations. This ¹⁵N T₁ reduction results in a corresponding 3-fold decrease of ¹⁵N polarization levels. These findings have substantial translational relevance for the rational design of hyperpolarized MRI contrast agents comprising ¹⁵N- and ¹³C-labeled biomolecules—both in general, and in the specific case of SABRE-hyperpolarized metronidazole, an antibiotic that can be potentially employed for non-invasive hypoxia sensing antibiotics,²⁰ emerging cancer therapeutics such as

evofosfamide²² and nimorazole radiosensitizers,²³ etc. Feasibility of high resolution MRI of HP metronidazole is shown, which bodes well for potential biomedical applications.

Conflicts of interest

BMG, EYC declare stake ownership in XeUS Technologies, LTD.

Acknowledgements

This work was supported by the NSF under grants CHE-1904780 and CHE-1905341, NIH R21CA220137, DOD CDMRP W81XWH-12-1-0159/BC112431, W81XWH-15-1-0271 and W81XWH-15-1-0272. O.G.S. thanks the RFBR (#19-33-60045) for the support of mechanistic studies with the use of parahydrogen. N.V.C. and K.V.K. thank the RFBR and Novosibirsk region government (#18-43-543023) for their support in the synthesis of ¹⁵N-labeled compounds. I.V.K. thanks the Russian Ministry of Science and Higher Education (project AAAA-A16-116121510087-5) and the RFBR (#19-29-10003, #17-54-33037) for financial support.

Notes and References

1. J. H. Ardenkjaer-Larsen, *J. Magn. Reson.*, 2016, **264**, 3-12.
2. K. V. Kovtunov, E. V. Pokochueva, O. G. Salnikov, S. Cousin, D. Kurzbach, B. Vuichoud, S. Jannin, E. Y. Chekmenev, B. M. Goodson, D. A. Barskiy and I. V. Koptyug, *Chem. Asian J.*, 2018, **13**, 1857-1871.
3. R. W. Adams, J. A. Aguilar, K. D. Atkinson, M. J. Cowley, P. I. P. Elliott, S. B. Duckett, G. G. R. Green, I. G. Khazal, J. Lopez-Serrano and D. C. Williamson, *Science*, 2009, **323**, 1708-1711.
4. P. J. Rayner and S. B. Duckett, *Angew. Chem. Int. Ed.*, 2018, **57**, 6742-6753.
5. M. J. Cowley, R. W. Adams, K. D. Atkinson, M. C. R. Cockett, S. B. Duckett, G. G. R. Green, J. A. B. Lohman, R. Kerssebaum, D. Kilgour and R. E. Mewis, *J. Am. Chem. Soc.*, 2011, **133**, 6134-6137.
6. R. A. Green, R. W. Adams, S. B. Duckett, R. E. Mewis, D. C. Williamson and G. G. R. Green, *Prog. Nucl. Mag. Res. Spectrosc.*, 2012, **67**, 1-48.
7. K. L. Ivanov, A. N. Pravdivtsev, A. V. Yurkovskaya, H.-M. Vieth and R. Kaptein, *Prog. Nucl. Mag. Res. Spectrosc.*, 2014, **81**, 1-36.
8. A. N. Pravdivtsev, A. V. Yurkovskaya, H. Zimmermann, H.-M. Vieth and K. L. Ivanov, *RSC Adv.*, 2015, **5**, 63615-63623.
9. A. N. Pravdivtsev, A. V. Yurkovskaya, H.-M. Vieth and K. L. Ivanov, *J. Phys. Chem. B*, 2015, **119**, 13619-13629.
10. J.-B. Hövener, A. N. Pravdivtsev, B. Kidd, C. R. Bowers, S. Glöggler, K. V. Kovtunov, M. Plaumann, R. Katz-Brull, K. Buckenmaier, A. Jerschow, F. Reineri, T. Theis, R. V. Shchepin, S. Wagner, P. Bhattacharya, N. M. Zacharias and E. Y. Chekmenev, *Angew. Chem. Int. Ed.*, 2018, **57**, 11140-11162.
11. D. A. Barskiy, K. V. Kovtunov, I. V. Koptyug, P. He, K. A. Groome, Q. A. Best, F. Shi, B. M. Goodson, R. V. Shchepin, M. L. Truong, A. M. Coffey, K. W. Waddell and E. Y. Chekmenev, *ChemPhysChem*, 2014, **15**, 4100-4107.
12. T. Theis, M. L. Truong, A. M. Coffey, R. V. Shchepin, K. W. Waddell, F. Shi, B. M. Goodson, W. S. Warren and E. Y. Chekmenev, *J. Am. Chem. Soc.*, 2015, **137**, 1404-1407.
13. M. L. Truong, T. Theis, A. M. Coffey, R. V. Shchepin, K. W. Waddell, F. Shi, B. M. Goodson, W. S. Warren and E. Y. Chekmenev, *J. Phys. Chem. C*, 2015, **119**, 8786-8797.
14. S. Duckett, S. Roy, P. Norcott, P. J. Rayner and G. G. R. Green, *Chem. Eur. J.*, 2017, **23**, 10496-10500.
15. A. M. Olaru, T. B. R. Robertson, J. S. Lewis, A. Antony, W. Iali, R. E. Mewis and S. B. Duckett, *ChemistryOpen*, 2018, **7**, 97-105.
16. D. A. Barskiy, R. V. Shchepin, C. P. N. Tanner, J. F. P. Colell, B. M. Goodson, T. Theis, W. S. Warren and E. Y. Chekmenev, *ChemPhysChem*, 2017, **18**, 1493-1498.
17. R. V. Shchepin, B. M. Goodson, T. Theis, W. S. Warren and E. Y. Chekmenev, *ChemPhysChem*, 2017, **18**, 1961-1965.
18. B. E. Kidd, J. L. Gesiorski, M. E. Gemeinhardt, R. V. Shchepin, K. V. Kovtunov, I. V. Koptyug, E. Y. Chekmenev and B. M. Goodson, *J. Phys. Chem. C*, 2018, **122**, 16848-16852.
19. R. V. Shchepin, J. R. Birchall, N. V. Chukanov, K. V. Kovtunov, I. V. Koptyug, T. Theis, W. S. Warren, J. G. Gelovani, B. M. Goodson, S. Shokouhi, M. S. Rosen, Y.-F. Yen, W. Pham and E. Y. Chekmenev, *Chem. Eur. J.*, 2019, **25**, 8829-8836.
20. K. Nepali, H.-Y. Lee and J.-P. Liou, *J. Med. Chem.*, 2018, **62**, 2851-2893.
21. K. Hendrickson, M. Phillips, W. Smith, L. Peterson, K. Krohn and J. Rajendran, *Radiother. Oncol.*, 2011, **101**, 369-375.
22. L. J. O'Connor, C. Cazares-Körner, J. Saha, C. N. G. Evans, M. R. L. Stratford, E. M. Hammond and S. J. Conway, *Org. Chem. Front.*, 2015, **2**, 1026-1029.
23. ClinicalTrials.gov, Clinical trial #NCT01507467.
24. R. B. Roy, S. M. Laird and L. Heasman, *Br. J. Vener. Dis.*, 1975, **51**, 281-284.
25. Y. Masaki, Y. Shimizu, T. Yoshioka, Y. Tanaka, K.-i. Nishijima, S. Zhao, K. Higashino, S. Sakamoto, Y. Numata, Y. Yamaguchi, N. Tamaki and Y. Kuge, *Sci. Rep.*, 2015, **5**, 16802.
26. J. Kurhanewicz, D. B. Vigneron, K. Brindle, E. Y. Chekmenev, A. Comment, C. H. Cunningham, R. J. DeBerardinis, G. G. Green, M. O. Leach, S. S. Rajan, R. R. Rizi, B. D. Ross, W. S. Warren and C. R. Malloy, *Neoplasia*, 2011, **13**, 81-97.
27. R. V. Shchepin, L. Jaigirdar, T. Theis, W. S. Warren, B. M. Goodson and E. Y. Chekmenev, *J. Phys. Chem. C*, 2017, **121**, 28425-28434.
28. R. V. Shchepin, L. Jaigirdar and E. Y. Chekmenev, *J. Phys. Chem. C*, 2018, **122**, 4984-4996.
29. T. Theis, N. M. Ariyasingha, R. V. Shchepin, J. R. Lindale, W. S. Warren and E. Y. Chekmenev, *J. Phys. Chem. Lett.*, 2018, **9**, 6136-6142.
30. P. Bernatowicz, D. Kubica, M. Ociepa, A. Wodyński and A. Gryff-Keller, *J. Phys. Chem. A*, 2014, **118**, 4063-4070.
31. J. W. Blanchard, T. F. Sjolander, J. P. King, M. P. Ledbetter, E. H. Levine, V. S. Bajaj, D. Budker and A. Pines, *Phys. Rev. B*, 2015, **92**, 220202.
32. D. A. Barskiy, A. N. Pravdivtsev, K. L. Ivanov, K. V. Kovtunov and I. V. Koptyug, *Phys. Chem. Chem. Phys.*, 2016, **18**, 89-93.
33. D. A. Barskiy, S. Knecht, A. V. Yurkovskaya and K. L. Ivanov, *Prog. Nucl. Mag. Res. Spectrosc.*, 2019, **114-115**, 33-70.
34. D. A. Barskiy, L. A. Ke, X. Li, V. Stevenson, N. Widarman, H. Zhang, A. Truxal and A. Pines, *J. Phys. Chem. Lett.*, 2018, **9**, 2721-2724.
35. R. E. Mewis, M. Fekete, G. G. R. Green, A. C. Whitwood and S. B. Duckett, *Chem. Comm.*, 2015, **51**, 9857-9859.
36. A. Manoharan, P. Rayner, W. Iali, M. Burns, V. Perry and S. Duckett, *ChemMedChem*, 2018, **13**, 352-359.

TOC Graphics

Presence of ^{14}N nucleus in the scalar coupling network causes deleterious effects in SABRE hyperpolarization in microtesla fields resulting in 3-fold decrease of ^{15}N T_1 and polarization values for all ^{15}N sites in $^{15}\text{N}_2$ -isotopologue versus $^{15}\text{N}_3$ -isotopologue.

